JOURNAL OF BIOMEDICAL OPTICS 4(3), 337–344 (JULY 1999)

COMPARATIVE STUDY OF LASER DAMAGE THRESHOLD ENERGIES IN THE ARTIFICIAL RETINA

Dale J. Payne,[†] Richard A. Hopkins, Jr.,[†] Brent G. Eilert,[†] Gary D. Noojin,[‡] David J. Stolarski,[‡] Robert J. Thomas,[‡] Clarence P. Cain,[‡] Gordon T. Hengst,[†] Paul K. Kennedy,[†] Thomas R. Jost,[†] and Benjamin A. Rockwell[†]

[†]Air Force Research Laboratory, Human Effectiveness Directorate, Directed Energy Bioeffects Division, Optical Radiation Branch, 8111 18th Street, Brooks AFB, Texas 78235-5215; [‡]TASC, 4241 Woodcock Drive, Suite B-100, San Antonio, Texas 78228-1330

(Paper JBO-207 received July 1, 1998; revised manuscript received Apr. 9, 1999; accepted for publication May 18, 1999.)

ABSTRACT

Laser damage threshold energies produced from ultrashort (i.e., $\leqslant$1 ns) laser pulses are investigated as a function of both pulse width and spot size for an artificial retina. A piece of film acts as the absorbing layer and is positioned at the focus of a variant on the Cain artificial eye [C. Cain, G. D. Noojin, D. X. Hammer, R. J. Thomas, and B. A. Rockwell, ''Artificial eye for *in vitro* experiments of laser light interaction with aqueous media,'' *J. Biomed. Opt.* **2**, 88–94 (1997)]. Experiments were performed at the focal point and at two and ten Rayleigh ranges (RR) in front of the focus with the damage end point being the presence of a bubble imaged at the film plane. Pulse energy thresholds were determined for wavelengths of 1064, 580, and 532 nm with pulse durations ranging from the nanosecond (ns) to the femtosecond (fs) regime. For the at-focus data in the visible regime, the threshold dropped from 0.25 μJ for a 532 nm, 5 ns pulse to 0.11 μJ for a 580 nm, 100 fs pulse. The near-infrared (NIR) threshold changed from 5.5 μJ for a 5 ns pulse to 0.9 μJ for a 130 fs pulse at a distance two RR in front of the focus. The experiment was repeated using the same pulse widths and wavelengths, except the water path was removed to determine the impact of nonlinear self-focusing in water. A vertical microscope imaging system was employed in order to observe the threshold event. The NIR fluence threshold of 0.5 J/cm^2 remained constant within an experimental uncertainty for all pulse widths, which corresponds to values in the literature [C. P. Lin and M. W. Kelly, ''Ultrafast time-resolved imaging of stress transient and cavitation from short pulsed laser irradiated melanin particles,'' *SPIE Laser-Tissue Interactions VI, Proc. SPIE* **2391**, 294–299 (1995)]. The visible data also demonstrated a nearly constant fluence of 0.07 J/cm^2. The disparity in thresholds between the two techniques arises from nonlinear optical phenomena related to propagation differences in the ocular fluid. *© 1999 Society of Photo-Optical Instrumentation Engineers.* [S1083-3668(99)01103-X]

Keywords ultrashort laser pulse; retina; cavitation; damage; threshold.

1 INTRODUCTION

Safety considerations of ultrashort laser pulses incident on the eye have been of great concern in recent years due to the increasing commercial availability of ultrashort pulse laser systems. Damage at or near the retina is of primary interest because of the retina's importance to visual function. However, damage mechanisms may be difficult to ascertain since numerous biological and physical processes are occurring in the eye, and these processes may either increase or lessen damage.[1–4] In order to understand the interaction between the laser pulse and the retina, but without the complications of a biological system, thresholds were measured on an artificial retina in an artificial eye for a variety of wavelengths, spot sizes, and pulse widths. In the experiment a piece of exposed camera film was used as the artificial retina, which simulates the granular absorber nature of the retinal pigmented epithelium (RPE). To further simplify study of the laser-retinal interaction, the effects of ocular focusing and propagation can be removed by focusing directly on the film, outside of the artificial eye.

2 EXPERIMENT

The experimental setup shown in Figure 1 was used to image cavitation events from the artificial retina in the artificial eye. Ultrashort laser system 1 contains a mode-locked (82 MHz) pulse compressed, frequency doubled Nd:yttrium–aluminum–garnet (YAG) laser used to excite a dye laser that produces a 580 nm beam. This beam is then amplified by a three-stage pulse dye amplifier

Address all correspondence to Benjamin A. Rockwell. Tel: 210-536-4790; Fax: 210-536-3903; E-mail: ben.rockwell@hedo.brooks.af.mil

1083-3668/99/$10.00 © 1999 SPIE

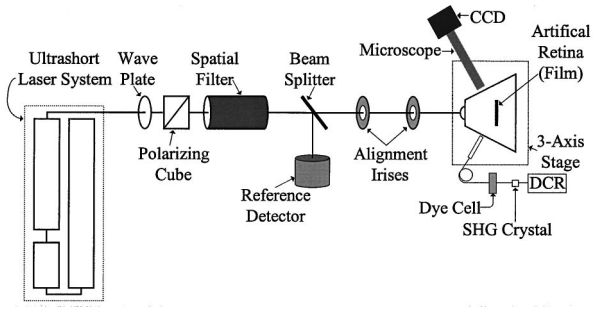

Fig. 1 Top view of the experimental setup for observing bubble formation from irradiated absorbing layer. Measurements in this setup allow for beam propagation in water before impinging the artificial retina.

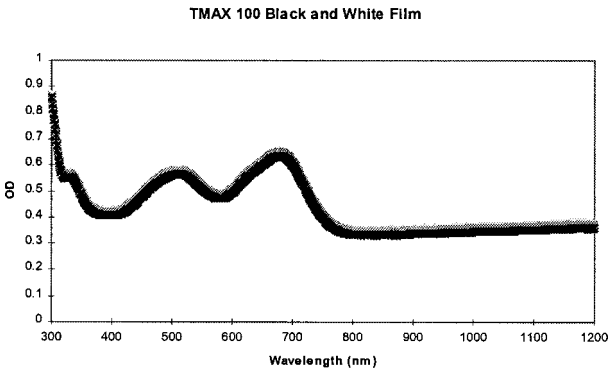

Fig. 2 Spectophotometric scan of film used as the artificial retina. The overlapping spectra verify sample homogeneity.

(PDA), with the PDA being pumped by a seeded, frequency doubled Nd:YAG regenerative amplifier. Upon exiting the PDA the laser light is directed through a spatial filter so that a Gaussian beam profile is achieved. Ultrashort laser system 1 produces 100 fs, 300 fs, and 3 ps pulses at 580 nm; 80 ps and 3 ns pulses at 532 nm; and 80 ps and 5 ns pulses at 1064 nm. Ultrashort laser system 2 (not shown) is an injection seeded Ti:sapphire regenerative amplifier. The seed beam is produced by an Ar^+ laser-pumped Ti:sapphire mode-locked oscillator. This beam is injected into the Ti:sapphire regenerative amplifier which is pumped by a high energy Nd:YAG laser. Laser system 2 was tuned to output at a wavelength of 1060 nm with a pulse duration of 130 fs.

A GLAN prism and a $\lambda/2$ wave plate are utilized to adjust the beam energy entering the spatial filter. Part of the beam is redirected by a beam splitter into a reference energy detector while the remainder of the light is focused onto the piece of film in the Cain artificial eye.[5] Another detector is placed in front of the Cain artificial eye so that the ratio between the reflected and reference beams is known. Thus, when the energy reading recorded by the reference detector is multiplied by the ratio, the energy reaching the artificial eye is known for every laser shot. Pulse widths were verified by either an Inrad slow-scan autocorrelator or fast photodiode and oscilloscope.

The process of threshold measurement consists of focusing a series of pulses of varying energies onto the artificial retina and observing the presence or absence of bubble formation. Holographic notch filters are used to block scattered or reflected laser light from obscuring the detection process. For each pulse width and wavelength, hundreds of data points are taken encompassing a range of pulse energies from subthreshold to suprathreshold values. Each data point consists of a reading by two observers on whether or not a particular pulse energy generated a bubble. The resulting data are analyzed using a statistical package known as SAS probit.[6] Threshold is then defined as the energy corresponding to 50% probability of bubble formation, the ED_{50}.

The type of film used in this experiment was Kodak black-and-white TMAX 100™. The silver halide granules had an average circular diameter of 1 μm and an average thickness of 0.16 μm. The film was exposed by directing a camera into a Hoffman integrating sphere to supply an even light illumination of the film, allowing for a uniform distribution of exposed particles. A calibrated LiteMate III photometer was placed at the exit port of the integrating sphere to determine the incident flux, and a value of 40 cd/m^2 was measured through the aperture. The film was exposed at an *f*-stop of 8 and an exposure time of 1/15 s. Particle counting revealed there were between three and five granules within a 10 μm by 10 μm area of the film. Analysis of the data yielded a mean value of 3.8 ± 0.5 using a 90% confidence level. To check the homogeneity of the film, two different pieces were examined using a spectrophotometer. In both cases the entire piece of film was scanned between 200 and 1200 nm. The results are shown in Figure 2, which is a plot of optical density versus wavelength. The overlap in spectra confirmed that particle distribution was consistent for the two film samples.

2.1 CASE 1: WATER FILLED ARTIFICIAL EYE

The artificial eye used in this experiment simulates the focusing characteristics of the rhesus monkey eye, and was designed and constructed in house. The lens, which has a 17 mm focal length, is embedded into the front face of the cuvette and was designed such that the lens-water interface minimizes aberration of the laser beam as it focuses in water. (The reader interested in learning more about aberrations will find a discussion in most standard optics texts.) The spot size (radius) of the laser measured in water at the beam waist is 2.5 μm for the visible wavelengths, and the cone angle is calculated to be 8°. Positioning of the film was accomplished by using three independent translation stages: two for rastering horizontally and vertically to align the film in the correct exposure location,

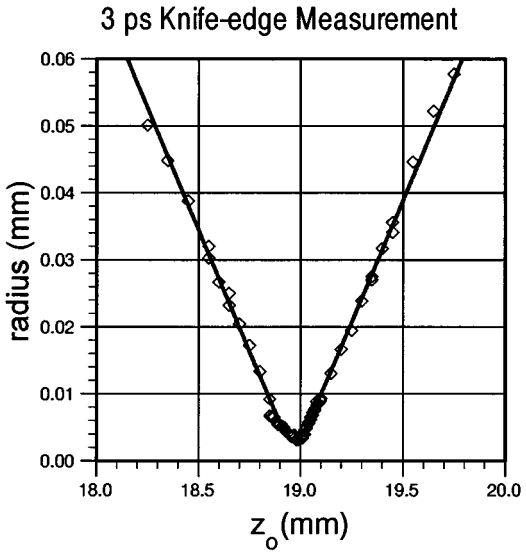

Fig. 3 Knife-edge measurement for a 3 ps 580 nm pulse.

and the third for bringing the film to the focal point of the artificial eye. Focusing of the film involved removing the holographic laser line filters from the video microscope geometry so that the laser beam is observable on the monitor. The beam spot size was measured and the film moved until the minimum diameter was achieved. The filters were then returned to the system to block the pump pulse.

The ultrashort laser pump pulse was delivered through the front of the artificial eye and focused onto the artificial retina. A probe laser pulse strobed the event 500 ns later and is recorded by a progressive scan Sony charge coupled device (CCD) camera, which has an 8.3 μm pixel size. The probe pulse came from a Q-switched frequency doubled Nd:YAG laser exciting Rhodamine 640 dye to fluoresce. The fluorescence was sent through a fiberoptic cable to illuminate the region of interest on the artificial retina. The light was brought in at an angle so that it reflected from the surface of the film and into the long working distance video microscope. This method allowed viewing of the reflected light from the film. The resolution of the system was 228 line pairs/mm according to factory specifications.

A micro-stepping stage controller was used to translate the film along the optical, scan, and vertical axes within the artificial eye. For the artificial eye setup, the knife-edge measurements were taken for each pulse duration and wavelength, and yielded a beam diameter of approximately 5 μm at focus. Figure 3 shows the result of a typical knife-edge measurement. The triangles are the recorded data and the solid line is the theoretical fit to the data using the equation

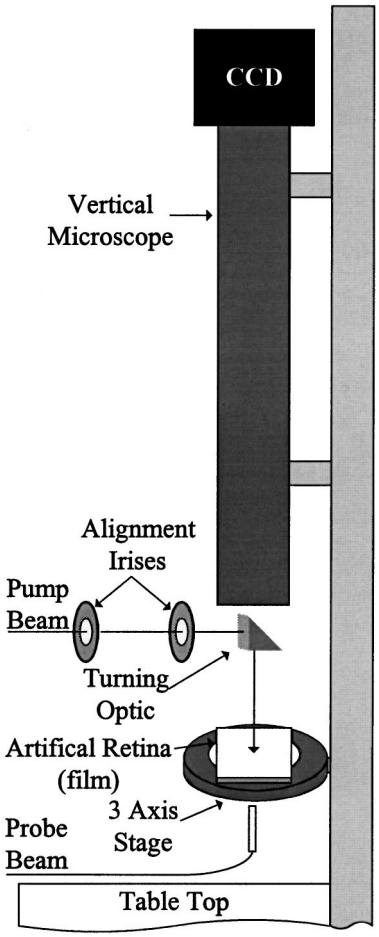

Fig. 4 Side view of experimental setup for observing bubble formation from irradiated absorbing layer.

$$r(z) = M^2 r_0 \left\{ 1 + \left[\frac{\lambda_n (z - z_0)}{\pi M^2 r_0^2} \right]^2 \right\}^{1/2}, \qquad (1)$$

where M^2 describes the deviation from a perfect Gaussian diffraction limit, r_0 is the diffraction-limited beam radius, and z is the position from the minimum radius position z_0.[5]

2.2 CASE 2: DRY ARTIFICIAL RETINA

Figure 4 illustrates the vertical microscope imaging system. It is essentially the same as the setup for the Cain artificial eye, except a single lens was used to focus the laser beam onto the absorbing layer without any water propagation path. In the case of the vertical microscope the focus of the objective was fixed and the sample was positioned using three micrometer driven stages. The objective itself has a long working distance (33.5 mm) and has a large numerical aperture (N.A.=0.28). The ultimate resolution of the objective is 1 μm according to the manufacturer, and was confirmed independently by our laboratory. Also the strobe illumination was brought in beneath the film, and again was timed to be 500 ns after the pump pulse delivery. The knife-

Table 1 Listed are the artificial retina damage thresholds for the water-filled cell. The NIR wavelength data are corrected to allow for the difference in focal length.

Pulse duration (ps)	Wavelength (nm)	ED_{50} (μJ)
5000	1064	5.51±0.45
80	1064	3.82±0.33
0.130	1060	0.90±0.05
3000	532	0.25±0.003
80	532	0.09±0.006
3.0	580	0.08±0.005
0.300	580	0.08±0.004
0.100	580	0.11±0.008

edge technique was used to measure the beam radius at the film plane in the vertical microscope studies. This provided us with an average $1/e^2$ Gaussian beam radius of 21 μm±2 μm for all pulse widths.

3 RESULTS

Thresholds were determined by SAS probit analysis[6] of the data. In the Case 1 optical configuration, it was observed that as the laser pulse width decreased, the threshold energy also decreased. For the at-focus data in the visible regime, the threshold dropped from 0.25 μJ for a 5 ns pulse at 532 nm to 0.11 μJ for a 100 fs, 580 nm pulse. An infrared pulse entering the eye focuses 400 μm behind the retina,[7] or in this case 400 μm behind the focal plane for visible light in the artificial eye. The visible pulse focal plane is thus two Rayleigh ranges (2RR) in front of the focal plane for the near-infrared (NIR)

Table 2 Listed are (a) the artificial retina damage thresholds and (b) the artificial retina beam radius for the water-filled cell as a function of distance from the focal plane.

(a) Artificial retina damage thresholds

Pulse duration (s)	Wavelength (nm)	At-focus ED_{50} (μJ)	2 RR ED_{50} (μJ)	10 RR ED_{50} (μJ)
5.00E-09	1064	0.59±0.11	5.51±0.45	N/A
8.00E-11	1064	0.26±0.01	3.82±0.33	N/A
1.30E-13	1060	0.24±0.002	0.90±0.05	18.8±0.8
3.00E-09	532	0.25±0.003	0.41±0.03	1.74±0.05
8.00E-11	532	0.09±0.006	0.13±0.01	0.61±0.05
3.00E-12	580	0.08±0.005	0.09±0.005	0.33±0.02
3.00E-13	580	0.08±0.004	0.13±0.03	0.89±0.03
1.00E-13	580	0.11±0.008	0.35±0.02	5.30±0.15

(b) Artificial retina beam radius

Pulse duration (s)	Wavelength (nm)	At-focus beam radius (μm)	2 RR beam radius (μm)	10 RR beam radius (μm)
5.00E-09	1064	4.7±0.6	61.1±7.3	304.6±36.6
8.00E-11	1064	4.7±0.6	61.1±7.3	304.6±36.6
1.30E-13	1060	9.1±1.1	41.5±5	202.7±24.3
3.00E-09	532	3.9±0.5	6.1±0.7	23.4±2.8
8.00E-11	532	3.3±0.4	5.3±0.6	21.1±2.5
3.00E-12	580	2.7±0.3	5.6±0.7	25±3
3.00E-13	580	2.9±0.3	5.9±0.7	26±3.1
1.00E-13	580	2.3±0.3	5.9±0.7	27.2±3.3

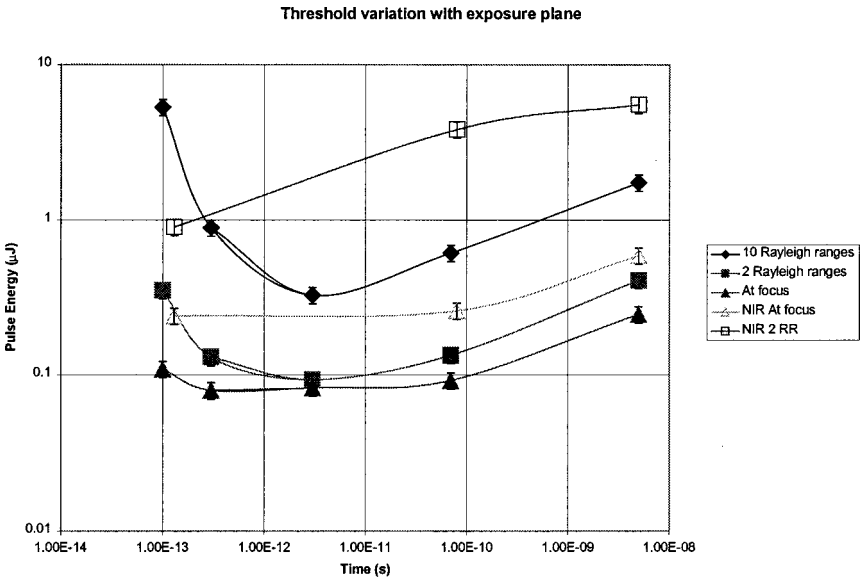

Fig. 5 Threshold energy trends for the visible and NIR wavelengths at focus (triangle), at 2 Rayleigh ranges (square), and at 10 Rayleigh ranges (diamond).

pulses. The near-IR thresholds at this 2RR plane varied from 5.5 μJ for a 5 ns pulse to 0.9 μJ for a 130 fs pulse. All the thresholds at the visible light focal plane are listed together for comparison in Table 1.

Table 2(a) lists all the ED_{50} values measured in the artificial eye as a function of distance from the focal plane. Thresholds were measured at the visible and NIR focal planes, as well as at 2RR and 10RR from these respective planes. Table 2(b) lists the spot sizes measured at each of the three planes, which increase as a function of distance from the focus. Threshold variation with distance from the focal plane is plotted in Figure 5. The trend lines in the graph are guides to the eye. Threshold energies for a particular pulse width and wavelength clearly increase with larger spot size. The trend in the threshold data as a function of increasing pulse width, however, seems approximately the same for visible exposures at three different planes and for NIR exposures at two different planes.

After completing the threshold measurements using the artificial retina in the artificial eye (Case 1), the experiment was repeated with the water path removed (Case 2). This aspect of the experiment was conducted for comparison with previous studies that were performed on isolated melanosomes that lack a substantial column of water above the melanosomes.[1] The vertical microscope system was used for observing bubble formation on the film as a result of laser impingement. The same criteria used previously for determining damage thresholds were also used in this part of the investigation. For the NIR data, the damage threshold fluence was measured to be approximately 0.5 J/cm^2 for all pulse widths, which is comparable to values reported by others[1] for bubble formation about melanosomes. The visible data also demonstrated a nearly constant fluence of 0.07 J/cm^2. An average beam radius of 22 μm was used to calculate the fluence for each pulse width. Because two separate wavelengths were used to obtain the visible trend, the results were normalized to the 532 nm wavelength. This was done by multiplying the ratio of the absorption coefficients for the artificial retina at 580 and 532 nm by the 580 nm damage threshold. These results are shown in Table 3 and plotted in Figure 6.

4 DISCUSSION

Previous experiments for determining minimum visible lesion (MVL) thresholds over the same spectral range and pulse duration have demonstrated a

Table 3 Artificial retina damage thresholds for Case 2.

Pulse duration (s)	Wavelength (nm)	ED_{50} (μJ)	Normalized ED_{50} (μJ)
5.00E-09	1064	8.96±0.57	···
8.00E-11	1064	7.13±0.94	···
1.30E-13[a]	1060	54.2±7	···
3.00E-09	532	1.03±0.07	···
8.00E-11	532	1.01±0.06	···
3.00E-12	580	1.61±0.05	1.39±0.05
3.00E-13	580	1.24±0.09	1.08±0.09
1.00E-13	580	0.82±0.07	0.71±0.07

[a] Spot size for this pulse width was 60 μm.

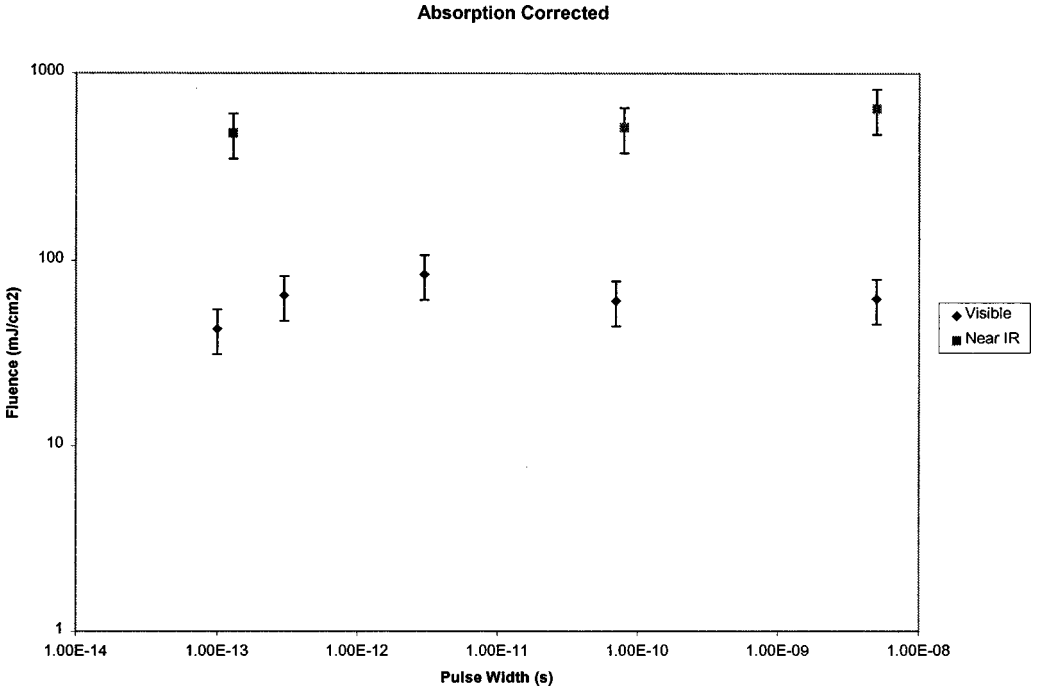

Fig. 6 Artificial retina threshold using the vertical microscope setup. The data illustrate the constant fluence measured.

similar trend to the thresholds measured in the artificial eye (Case 1). In Case 1, we determined that less energy is required for retinal damage as the pulse width decreases.[8] Rockwell et al.[7,9] have suggested that for pulses with nanosecond to microsecond durations the primary damage mechanism is photomechanical (bubble formation about melanosomes). This is because the absorbing material has insufficient time to conduct heat away from itself during energy deposition. Rockwell et al.[10] and Cain et al.[11] have suggested that self-focusing, and perhaps laser induced breakdown (LIB), occur in the eye for femtosecond pulses. They performed *in vivo* MVL studies on both rabbit and rhesus monkey eyes, and concluded that self-focusing and LIB were contributors to lesion formation. Therefore, self-focusing may have occurred in the artificial retina investigations, reducing the amount of energy required to cause damage. Cain et al.[11] also calculated that for a 100 fs pulse in the visible regime, the LIB threshold for a water-filled artificial eye is 0.27 μJ. The present study used the same pulse width and wavelength, but measured a threshold of 0.109 μJ for damage, less than half the LIB threshold. The conclusion is that LIB was not a participant in this study, but self-focusing is likely to have reduced the damage thresholds for Case 1.

Our measurements for Case 2 show a pulse width independent damage threshold for the artificial retina as the pulse duration is reduced from several nanoseconds to 100 fs. Microsecond to femtosecond laser pulse studies on skin[12–15] have also demonstrated the pulse width independent nature of radiant exposure thresholds. Energy deposition resulted in immediate whitening and ultrastructural alterations of melanosomes in black guinea pig skin, which formed the basis for threshold determination.[12] The skin experiments and those of Case 2 share a common aspect in that both were conducted in the absence of an intermediate water layer.

To confirm statistical validity of the trends, an analysis was performed in order to incorporate the uncertainties in the experimental measurements. The basic equation for average fluence will be defined as

$$H = \frac{Q}{\pi r^2}, \tag{2}$$

where H is the average fluence over a $1/e^2$-Gaussian diameter laser profile, Q is the energy per pulse, and r is the $1/e^2$ radius of the beam. Thus, the total uncertainty takes into account the detector uncertainty and any uncertainty arising from measured quantities. After taking the appropriate partial derivatives and substituting in the known uncertainty values, an overall uncertainty in fluence of 27% was calculated for the vertical microscope experiment. Since the knife-edge scans done inside the artificial eye used stepper motors instead of manually adjusted micrometer stages, there was a 12% uncertainty in fluence for these measurements.

Figure 7 shows a plot of the MVL ED_{50} thresholds measured for visible and NIR ultrashort pulses.

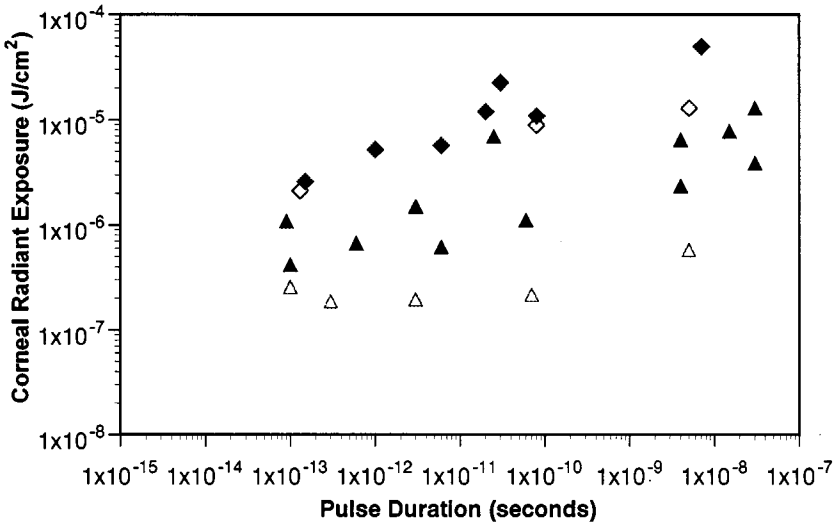

Fig. 7 Comparison between artificial retina thresholds (open symbols) and *in vivo* MVL thresholds (filled symbols). The diamonds represent NIR data points and the triangles are for visible wavelengths.

This figure illustrates how closely the artificial retina data (which lack any biological components), resembled the data taken using a biological system. This indicates that the underlying physics responsible for damaging the artificial retina within the artificial eye is the same as that responsible for damaging the biological retina of a normal eye. Furthermore, the extent of agreement between the two separate systems indicates that the artificial retina is a good emulator of the interaction between ultrashort laser pulses and the biological retina. An advantage here is that it can now be possible to construct models that explain the damage mechanism(s), but do not necessarily rely on biological contributions.

5 CONCLUSIONS

We have measured the energy thresholds necessary for bubble formation on an artificial retina in an artificial eye. For the at-focus data in the visible regime, the threshold dropped from 0.25 μJ for a 5 ns pulse at 532 nm to 0.11 μJ for a 580 nm, 100 fs pulse. At two Rayleigh ranges, the NIR (1064 nm) threshold changed from 5.5 μJ for a 5 ns pulse to 0.9 μJ for a 130 fs pulse. The trends observed in this study are similar to trends reported by Cain et al. for experiments performed on biological systems. This indicates that the artificial retina system approximates the physical response of a biological retina when exposed to laser pulses spanning nanosecond to femtosecond durations. However, we believe that to extract a complex mathematical function is beyond the scope of this paper and offers no benefit. There is no replacement for *in vivo* studies since all research pertaining to MVL thresholds must use the same model so that current experimental results can be directly linked to previous findings spanning the last thirty years.

Other authors have investigated the pulse width dependent nature of threshold in melanin. Experiments done on isolated melanosomes[2] and *in vitro* RPE cells[16] with no intervening water layer have indicated that the threshold remains the same, irrespective of pulse width. This is different than experiments performed on rhesus monkey eyes where it has been shown that for pulse durations between the nanosecond to femtosecond regimes the threshold does not remain constant. From our investigations using the artificial retina we have found that the differences reflect nonlinear optical processes arising from beam propagation through the eye. There must be a sufficiently long column of water present before these nonlinear processes, i.e., self-focusing and LIB, can manifest themselves. Due to resolution limitations, isolated melanosome experiments are typically conducted with only a thin layer of water covering the particle. This prohibits the development of nonlinear effects, and is responsible for the constant threshold observed. These results underscore the necessity of studying the influence propagation has on the damage mechanism(s).

Acknowledgments

This research was sponsored by the Air Force Office of Scientific Research (2312A103) and Air Force Research Laboratory, Armstrong Research site. This research was conducted while Dale Payne held an NRC-AFRL Postdoctoral Research Associateship.

REFERENCES

1. C. P. Lin and M. W. Kelly, ''Ultrafast time-resolved imaging of stress transient and cavitation from short pulsed laser irradiated melanin particles,'' *SPIE Laser-Tissue Interactions VI, Proc. SPIE* **2391**, 294–299 (1995).
2. R. D. Glickman and K-W Lam, ''Melanin may promote photooxidation of linoleic acid,'' in Ref. 1, p. 254.
3. T. Sarna, ''Properties and function of the ocular melanin—A photobiophysical view,'' *J. Photochem. Photobiol., B* **12**, 215 (1992).
4. H. C. Longuet-Higgins, ''On the origin of the free radical property of melanins,'' *Arch. Biochem. Biophys.* **86**, 231 (1960).
5. C. Cain, G. D. Noojin, D. X. Hammer, R. J. Thomas, and B. A. Rockwell, ''Artificial eye for *in vitro* experiments of laser light interaction with aqueous media,'' *J. Biomed. Opt.* **2**, 88–94 (1997).
6. SAS Institute, 1996, SAS probit procedure, Cary, NC.
7. B. A. Rockwell, D. X. Hammer, P. K. Kennedy, R. Amnotte, B. Eilert, J. J. Drussel, D. J. Payne, S. Phillips, D. J. Stolarski, G. D. Noojin, R. J. Thomas, and C. P. Cain, ''Retinal spot size with wavelength,'' *SPIE Laser-Tissue Interactions VIII, Proc. SPIE* **2975**, 147–154 (1997).
8. C. P. Cain, C. A. Toth, G. D. Noojin, D. J. Stolarski, and B. A. Rockwell, ''Femtosecond laser pulses in the near-infrared produces visible lesions in the primate eye,'' in *Laser–Tissue Interaction, Tissue Optics, and Laser Welding III*, Guy P. Delacretaz, Lars O. Svaas, Rudolf W. Steiner, Roberto Pini, and Guilheim Godlewski, Eds., *Proc. Spie* **3195**, 121–126 (1998).
9. D. Sliney and M. Wolbarsht, *Safety with Lasers and Other Optical Sources*, Chap. 4, Plenum Press, New York, NY (1985).
10. B. A. Rockwell, W. P. Roach, and M. E. Rogers, ''Determination of self-focusing effects for light propagating in the eye,'' *SPIE Laser-Tissue Interactions V, Proc. SPIE* **2134**, 2–9 (1994).
11. C. P. Cain, C. D. DiCarlo, B. A. Rockwell, P. K. Kennedy, G. D. Noojin, D. J. Stolarski, D. X. Hammer, C. A. Toth, and W. P. Roach, ''Retinal damage and laser-induced breakdown produced by ultrashort-pulse lasers,'' *Graefe's Arch. Clin. Exp. Ophthalmol.* **234**, 28–37 (1996).
12. S. Watanabe, R. R. Anderson, S. Brorson, G. Dalickas, J. G. Fujimoto, and T. J. Flotte, ''Comparative studies of femtosecond to microsecond laser pulses on selective pigmented cell injury in skin,'' *Photochem. Photobiol.* **53**, 757–762 (1991).
13. R. R. Anderson, R. J. Margolis, S. Watanabe, T. J. Flotte, G. J. Hruza, and J. S. Dover, ''Selective photothermolysis of cutaneous pigmentation by *Q*-switched Nd:YAG laser pulses at 1064, 532, and 355 nm,'' *J. Invest. Dermatol.* **93**, 28–32 (1989).
14. L. L. Polla, R. J. Margolis, J. S. Dover, D. Whitaker, F. G. Murphy, S. L. Jacques, and R. R. Anderson, ''Melanosomes are a primary target of *Q*-switched ruby irradiation in guinea pig skin,'' *J. Invest. Dermatol.* **89**, 281–286 (1987).
15. A. K. Tong, O. T. Tan, J. Boll, J. A. Parrish, and G. F. Murphy, ''Ultrastructrual effects of melanin pigment on target specificity using pulsed dye laser (577 nm),'' *J. Invest. Dermatol.* **88**, 747–752 (1987).
16. M. W. Kelly and C. P. Lin, in Ref. 7, pp. 174–179.